NASA TECHNICAL NOTE

NASA TN D-7850

NASA TN D-7850

NATIONAL AERONAUTICS AND SPACE ADMINISTRATION
U.S.A.

USE OF POTENTIAL FLOW THEORY TO EVALUATE SUBSONIC INLET DATA FROM A SIMULATOR-POWERED NACELLE AT CRUISE CONDITIONS

Lawrence J. Bober

Lewis Research Center
Cleveland, Ohio 44135

AMERICAN REVOLUTION BICENTENNIAL 1776-1976

NATIONAL AERONAUTICS AND SPACE ADMINISTRATION • WASHINGTON, D. C. • DECEMBER 1974

1. Report No. NASA TN D-7850	2. Government Accession No.	3. Recipient's Catalog No.
4. Title and Subtitle USE OF POTENTIAL FLOW THEORY TO EVALUATE SUBSONIC INLET DATA FROM A SIMULATOR-POWERED NACELLE AT CRUISE CONDITIONS		5. Report Date December 1974
		6. Performing Organization Code
7. Author(s) Lawrence J. Bober		8. Performing Organization Report No. E-7472
		10. Work Unit No. 501-24
9. Performing Organization Name and Address Lewis Research Center. National Aeronautics and Space Administration Cleveland, Ohio 44135		11. Contract or Grant No.
		13. Type of Report and Period Covered Technical Note
12. Sponsoring Agency Name and Address National Aeronautics and Space Administration Washington, D.C. 20546		14. Sponsoring Agency Code
15. Supplementary Notes		

16. Abstract

Incompressible potential flow theory corrected for compressibility effects, using the Lieblein-Stockman compressibility correction, was used to predict surface and flow field static pressures for a subsonic inlet at cruise conditions. The calculated internal and external surface static pressures were in good agreement with data at most conditions. The analysis was used to determine the capture stream-tube location and static-pressure distribution. Additive drag coefficients obtained from these results were consistently higher than those obtained using one-dimensional compressible flow theory. Increasing the distance between the inlet and boattail increased the cowl drag force. The effect of the boundary layer on internal and external surface static-pressure distributions was small at the design cruise condition. The analytical results may be used as an aid to data reduction and for predicting inlet mass flow, stagantion point location, and inlet additive drag.

17. Key Words (Suggested by Author(s)) Engine inlets Nacelles Inlet flow Pressure distribution Potential flow Additive drag	18. Distribution Statement Unclassified - unlimited Category 01		
19. Security Classif. (of this report) Unclassified	20. Security Classif. (of this page) Unclassified	21. No. of Pages 25	22. Price* $3.00

USE OF POTENTIAL FLOW THEORY TO EVALUATE SUBSONIC INLET DATA

FROM A SIMULATOR-POWERED NACELLE AT CRUISE CONDITIONS

by Lawrence J. Bober

Lewis Research Center

SUMMARY

Incompressible potential flow theory corrected for compressibility effects using the Lieblein-Stockman compressibility correction was used to predict surface and flow-field static pressures for a subsonic inlet at cruise conditions. The calculated surface static pressures were in good agreement for the internal cowl surface at inlet mass flows where local velocities were less than sonic and for the external surface at mass flows and free-stream Mach numbers where local velocities were only slightly greater than sonic. The analysis was used to determine the capture stream-tube location and static-pressure distribution. Additive drag coefficients obtained from these results were consistently higher than those obtained using one-dimensional compressible flow theory. Increasing the distance between the inlet and boattail increased the cowl drag force. The effect of the boundary layer on internal and external surface static-pressure distributions was small at the design cruise Mach number of the inlet investigated.

The application of the analytical results as an aid to data reduction was demonstrated and was found to be useful for predicting inlet weight flow, stagnation point location, and inlet additive drag. The analysis also indicated an interaction between the inlet and boattail flow fields for the experimental configuration.

INTRODUCTION

The use of turbofan simulators for wind-tunnel tests of nacelles for subsonic aircraft offers advantages over either flow-through nacelles (refs. 1 and 2) or separate tests of inlets (ref. 3) and boattails (refs. 4 and 5). Unfortunately, accurate determination of fan mass flow rate without extensive flow-field instrumentation is difficult for simulator powered nacelles. Since inlet and nacelle performance are usually presented as a function of mass flow ratio, accurate knowledge of the mass flow rate is required.

Determination of nacelle and, particularly, inlet performance depend on knowledge of the inlet additive drag. Since this parameter cannot be measured directly, it has been calculated from one-dimensional compressible flow theory (refs. 6 and 7). This calculation depends on the mass flow rate and the location of the stagnation point, which is also difficult to determine experimentally.

The objective of the investigation reported herein was to demonstrate the use of incompressible flow theory corrected for compressibility effects to increase the understanding of data obtained from wind tunnel tests of a simulator powered nacelle at cruise conditions.

To determine the simulator fan flow rate, analytically predicted internal cowl surface static pressures can be compared with measured values. Comparison of calculated and experimentally determined internal pressure distributions are shown for several fan flow rates up to the choking value at free-stream Mach numbers from 0.60 to 0.85 and at zero angle of attack. Theoretical pressure distributions on the cowl external surface are compared with data. The effect of the boundary layer on the calculated pressure distribution is presented. Calculated and measured stagnation point locations are shown for a range of flow rates and Mach numbers. The effect of inlet-boattail spacing on the cowl suction force is presented. Theoretical additive drag values are compared with one-dimensional values for a range of mass flow rates at Mach numbers from 0.60 to 0.85.

SYMBOLS

A	cross-sectional area
$C_{D, add}$	additive drag coefficient
$C_{D, cowl}$	external cowl drag coefficient
$C_{D, inl}$	inlet drag coefficient
D_{add}	additive drag
D_{cowl}	external cowl drag
D_{inl}	inlet drag
D_{max}	maximum nacelle diameter (54.61 cm)
L	axial distance from inlet highlight to diffuser exit (28.16 cm)
l	length of cylindrical section between inlet and boattail
M	Mach number
m	mass flow through the inlet

2

m_0 mass flow at free-stream conditions through an area equal to the maximum na-
celle cross-sectional area

P   total pressure

p   static pressure

V   velocity

X   length of external forebody (9.56 cm)

x   axial distance measured from inlet highlight

γ ratio of specific heats

ρ density

ϕ circumferential angle around inlet

Subscripts:

c   compressible

i   incompressible

isol   isolated inlet

l local

s   stagnation point

0   free stream

Superscripts:

-     average or one-dimensional

*   sonic

METHOD OF ANALYSIS

Analytical Methods

The potential flow analysis used in this study was the Douglas method (ref. 8) for
incompressible flow about axisymmetric bodies. Two basic solutions (ref. 9) were
combined to obtain arbitrary inlet mass flow rates for the zero-angle-of-attack condi-
tions considered in this study.

Since high subsonic Mach numbers are achieved by the flow over much of an inlet at
cruise conditions, compressibility effects must be taken into account in the analysis.
The empirical compressibility correction developed by Lieblein and Stockman (ref. 10)
for internal flows was applied to the incompressible results. The compressible velocity

in this method is given by

$$V_c = V_i \left(\frac{\rho_i}{\overline{\rho}_c} \right)^{V_i / \overline{V}_i} \tag{1}$$

where V_c is the local compressible velocity, V_i is the local incompressible velocity, ρ_i is the incompressible density (equal to the stagnation density), $\overline{\rho}_c$ is the local, one-dimensional compressible density (as used in this study), and $\overline{V}_i$ is the local, one-dimensional, incompressible velocity. This compressibility correction gave good results at takeoff and landing conditions (refs. 11 and 12). For the external flow on the surface starting at the stagnation point, $\overline{\rho}_c$ was taken to be the free-stream density, and the incompressible free-stream velocity was used for $\overline{V}_i$. Thus the compressible velocity in this region is given by

$$V_c = V_i \left(\frac{\rho_i}{\rho_0} \right)^{V_i / V_{i,0}} \tag{2}$$

This correction for the external surface is similar to the one used by Albers and Stockman (ref. 13).

The capture stream tube (fig. 1) was located in an iterative manner by applying the compressibility correction to points in the flow field ahead of the inlet as though the capture stream tube were a solid surface. At each axial location ahead of the inlet, where a row of off-body points was included in the incompressible analysis, the following calculations were performed:

(1) Assuming the compressible velocity at each point to be equal to the incompressible velocity, the density at each point was computed and the mass flux was integrated outward from the inlet centerline until the integrated mass flow was equal to the inlet mass flow (input to the program). This gave an initial estimate of the radial location of the capture stream tube.

(2) Using the current estimate for the location of the capture stream tube and treating the capture stream tube as a solid surface, the incompressible velocities at each point were corrected for compressibility using equation (1).

(3) Densities at each point were calculated using the velocities calculated in item (2) and the mass flux integrated as in item (1) to get a new location for the capture stream tube.

(4) The calculations in items (2) and (3) were repeated until satisfactory convergence was obtained for the location of the capture stream tube.

Using the location of and the velocity on the capture stream tube at each row of off body points, the additive drag was obtained by integrating spline fit curves of these variables.

Inlet boundary layers were investigated using the method of Herring and Mellor (ref. 14). The boundary-layer calculations were started using the option for plane stagnation-point flows. The effect of the boundary layer on the inlet-pressure distribution was determined by adding the displacement thickness to the body and recalculating the potential flow about this new body.

Since the configuration analyzed in this report consisted externally of the inlet followed by a cylindrical section and a boattail region, these regions were included in the analysis so that the effect of the boattail on the inlet would be reflected in the theoretical results.

Determination of Mass Flow Ratio

The mass flow ratio at which an engine is operating can be determined by comparing the experimentally measured inlet internal pressure distribution for which the mass flow ratio is not known to a series of theoretical pressure distributions for which the mass flow ratios are known (fig. 2). Comparison of the experimental pressure distribution with the theoretical pressure distributions shown in figure 2 indicate a mass flow ratio of approximately 0.660. For the same set of data, mass flow ratios determined from other, more conventional methods (one-dimensional flow theory) were 0.651, 0.685, and 0.696. In adapting this method to computer data reduction, one or more pressure taps (whose readings fall very nearly on the theoretical curve which "best" fits the data) are used to determine the mass flow ratio from an analytically determined tabulation of corrected weight flow against static-to-total pressure at the selected pressure tap. In choosing a pressure tap for determining weight flow, consideration should be given to locations where boundary-layer effects are negligible, where the static pressure is a strong function of weight flow, and, as mentioned previously, where theoretical and experimental pressures are in good agreement. For the data shown in this report and in reference 15, which reports on the experimental program, mass flow ratios were determined from static-pressure taps located at $x/L = 0.158$ and 0.278.

GEOMETRY

The experimental results shown in this report were obtained in the wind tunnel test described in references 15 and 16. A sketch of the model is shown in figure 3. The nacelle contains a turbofan simulator designed for a fan pressure ratio of 1.15.

5

Details of the inlet geometry to which the analysis was applied are shown in figure 4.
The inlet external forebody is an NACA 1 series contour (ref. 3) with a highlight to maximum diameter ratio of 0.935 and a forebody length to maximum diameter ratio of 0.175.
Based on the correlation of reference 17, this inlet has a drag divergence Mach number
of 0.80 at a mass flow ratio based on maximum nacelle projected area of 0.65. The internal contour from the highlight to the throat is a 2:1 ellipse having a contraction ratio
of 1.26.

DISCUSSION OF RESULTS

Surface Static Pressure Distributions

Internal pressure distributions. - The following comparisons of theoretical and experimental cowl internal pressure distributions demonstrate that reasonable results can
be obtained when mass-flow ratios are determined in an experimental program by using
the method discussed previously.

Figure 5 shows three sets of experimental inlet internal pressure distributions together with the analytically predicted pressure distributions, which yielded the indicated
mass-flow ratios. The free-stream Mach number for all three cases was 0.60. The
agreement is very good in figures 5(a) and (b) where the flow is entirely subsonic, but
in figure 5(c) the agreement is not as good in the first 50 percent of the inlet length.
This is apparently due to the extensive region of supersonic flow which exists in the inlet at this (choked) condition.

Comparisons of theoretical and experimental internal cowl pressure distributions
are shown in figures 6 and 7 for free-stream Mach numbers of 0.75 and 0.85, respectively. At the lower mass flow ratios shown in figures 6(a) and (b) and 7(a) and (b) the
agreement is very good. However, in figures 6(c) and 7(c) where comparisons are made
for the inlet choked, results are similar to those shown in figure 5(c) for $M_0 = 0.60$.

An indication of the accuracy of the present method for determining mass-flow ratio
can be obtained by comparing the mass-flow ratio at which the inlet choked (figs. 5(c),
6(c), and 7(c)) with the values obtained from one-dimensional, compressible flow theory.
For free-stream Mach numbers of 0.60, 0.75, and 0.85, the one-dimensional choking
mass flow ratios are 0.799, 0.714, and 0.686. The mass-flow ratios indicated in figures 5(c), 6(c), and 7(c) are an average of 2.4 percent lower than the one-dimensional
choking values. This difference is probably due to pressure gradients, in a direction
normal to the flow, which reduce the maximum mass flow that can pass through a given
area to a value less than the one-dimensional value.

In general, the theoretical internal pressure distributions agreed very well with the
experimental pressure distributions from the highlight to $x/L = 0.8$ at free-stream

Mach numbers between 0.60 and 0.85 and for all mass-flow ratios where no local super-
sonic flow was observed inside of the inlet. At all free-stream Mach numbers and
mass-flow ratios, a slight discrepancy was present near the fan face.

External pressure distributions. - Comparisons of theoretical and experimental
cowl surface static-pressure distributions are shown in figure 8 for a free-stream Mach
number of 0.60 at the same mass flow ratios shown in figure 5. (The mass-flow ratios
were determined as described previously using the measured internal cowl pressures
and the theoretical pressure distributions.) The theory accurately predicts the minimum
pressure on the external cowl, although the location of the minimum pressure as indica-
ted by the theory is slightly upstream of the location indicated by the data. At the lowest
mass-flow ratio conditions (fig. 8(a)) shown, the maximum surface Mach number indica-
ted by the theory was 1.28; the maximum value indicated by the data was 1.27.

At a free-stream Mach number of 0.75, the agreement between the theoretical and
experimental external cowl surface static-pressure distributions as shown in figure 9 is
not as good as those shown in figure 8 for a free-stream Mach number of 0.60. At the
low mass-flow condition shown in (fig. 9(a)), large discrepancies between the theoretical
and experimental pressure distributions were present from the highlight $(x = 0)$ to
$x/X = 0.3$ (or maybe 0.4). The local Mach numbers in this region (except for a small
region near the highlight) as determined from the data were supersonic with a maximum
value of 1.60. The maximum Mach number indicated by the theory was considerably
higher, about 2.26. Downstream of this region, where local Mach numbers were 1.03
or less $(x/X \geq 0.48)$, agreement was very good. As the mass-flow ratio was increased
(fig. 9(b)), agreement improved; at the highest mass flow condition (fig. 9(c)), agree-
ment was nearly as good as at $M_0 = 0.60$. Figure 9(c) shows the theoretical and experi-
mental pressure distributions at the choking mass-flow ratio. Only in a small region
near the highlight is there any significant discrepancy between the theoretical and ex-
perimental results.

The discrepancies noted near the highlight at a free-stream Mach number of 0.60
(fig. 8) and at the highest mass-flow ratio condition at a free-stream Mach number of
0.75 (fig. 9(c)) might be due to the coordinates used to represent the inlet in the potential
flow calculation. These coordinates were not obtained from measurements of the inlet
model but from specifications for construction of the model. Inspection of the model
after performing the calculations indicated deviations from the specifications near the
inlet highlight. These deviations might have been sufficient to cause the observed dis-
crepancies between the theoretical and experimental pressure distributions near the
highlight. Calculations using the actual inlet geometry were not performed since insuf-
ficient measurements were made to adequately define the actual inlet geometry.

The discrepancies noted at the lower mass-flow ratios for a free-stream Mach num-
ber of 0.75 could be caused by the inability of the analysis to adequately predict the flow

where local Mach numbers are considerably greater than 1.0 or by the presence of a region of separated flow on the cowl.

Theoretical and experimental external cowl surface static-pressure distributions at a free-stream Mach number of 0.85 are shown in figure 10. At this Mach number, which is above the design drag divergence Mach number, the theory represented poorly the actual flow for all mass-flow ratios at which calculations were performed. Even at the highest mass-flow ratio (inlet choked; fig. 10(c)), where the agreement was expected to be best, the theory and experimental results disagreed over the entire external surface of the inlet. This is not surprising since both the theoretical and experimental results indicate supersonic flow over the entire surface except for a small region near the highlight, and it is unreasonable to expect a subsonic analysis to accurately predict such a flow

Effect of boundary layer. - Boundary-layer effects on the cowl pressure distributions were investigated primarily to determine the accuracy of the procedure used to determine the inlet mass-flow ratio. Thus an extensive study of boundary-layer effects was not performed.

An attempt was made to use the laminar to turbulent transition correlation of Smith (ref. 18) as given by Cebeci, Mosinskis, and Smith (ref. 19) for the internal and external boundary-layer calculations. However, the boundary-layer analysis indicated laminar separation before transition was predicted. As a result, transition was assumed to occur just upstream of the indicated laminar separation point. Turbulent separation, as indicated by zero skin friction, was not encountered in this study.

The effect of boundary-layer growth on the internal and external cowl pressure distributions is shown in figure 11. The free-stream Mach number and inlet mass-flow ratio in figure 11(a) are approximately equal to the design cruise conditions for the inlet. Internally, the boundary-layer effect was negligible from the highlight to slightly downstream of the throat or at about $x/L = 0.3$. Externally, there was no appreciable effect on the inlet portion of the contour which ended at approximately $x/L = 0.3$. Accounting for the boundary layer causes decreases in local pressures of less than 1 percent with the maximum effect occurring internally at the diffuser exit.

The effect of the boundary layer on the cowl pressure distribution is shown in figure 11(b) for the theoretical choking condition in the inlet at free-stream Mach 0.75. Internally, the choked flow condition has the most severe adverse pressure gradients, causing the thickest boundary layers and the largest deviations from the inviscid pressure distributions. Internally, the boundary-layer effect was negligible upstream of the throat $(x/L = 0.198)$, caused about a 2-percent decrease in pressure at the diffuser exit, and caused a maximum decrease in pressure of about 4 percent at about $x/L = 0.42$. Externally, there was no appreciable effect on the inlet pressure distribution.

Stagnation-point location. - Accurate knowledge of the stagnation-point location is important because it defines the starting point for the pressure integration, which determines the cowl suction force. One-dimensional additive drag calculations also require

8

knowledge of the stagnation-point location. The effects of mass-flow ratio and free-stream Mach number on the theoretical and experimental stagnation-point locations are presented in figure 12. The analysis indicated that the stagnation-point location at a fixed mass-flow ratio was independent of free-stream Mach number for the range 0.60 to 0.85. The agreement between the theoretical and experimental stagnation-point locations is reasonable, although the experimentally determined locations were consistently closer to the inlet highlight on the internal surface of the cowl. As noted previously this could be due to discrepancies between the actual inlet coordinates and those used in the analysis.

Capture stream-tube pressure distributions. - Figure 13 is a comparison of typical capture stream-tube pressure distributions calculated from the two-dimensional analysis described previously and from one-dimensional compressible flow theory. The ratio of static-to-total pressure at the stagnation point as calculated from one-dimensional theory is considerably less than the actual stagnation value of 1.0.

<div align="center">Inlet Forces</div>

The cowl drag force D_{cowl} is determined by integrating the difference between the local surface static pressure and the free-stream static pressure from the stagnation point to the location of the maximum nacelle diameter. The cowl drag force is thus given by

$$D_{cowl} = \int_{A_s}^{A_{max}} (p_l - p_0)dA$$

The additive drag D_{add} is determined by integrating the difference between the local static pressure on the capture stream tube and the free-stream static pressure from free-stream conditions upstream of the inlet to the stagnation point on the inlet surface. This can be written as

$$D_{add} = \int_{A_0}^{A_s} (p_l - p_0)dA$$

The inlet drag D_{inl} is the sum of the cowl drag and additive drag,

$$D_{inl} = D_{cowl} + D_{add}$$

These terms are made dimensionless by dividing them by the product of the free-stream dynamic pressure $\frac{1}{2}\gamma p_0 M_0^2$ and the maximum nacelle cross-sectional area A_{max} and

are thus denoted by $C_{D,cowl}$, $C_{D,add}$ and $C_{D,inl}$.

Cowl drag. - The effects of mass-flow ratio and free-stream Mach number on the theoretical and experimental cowl drag coefficients are shown in figure 14. Both indicate that the cowl drag coefficients are weak functions of Mach number at Mach 0.79 or less. At a free-stream Mach number of 0.85 the experimental cowl drag coefficients are lower than at the lower free-stream Mach numbers. Since the design drag divergence Mach number of the inlet is 0.80, this behavior is reasonable. The theoretical results at a free-stream Mach number of 0.85 are at about the same level as the theoretical results at the lower free-stream Mach numbers, since the inviscid, subsonic analysis used in this study does not consider the effects that cause drag divergence. Although the pressure distributions shown in figures 9(a) and (b) indicate significant discrepancies between the theory and the data, the theoretical and experimental cowl drag coefficients of figure 14 are in reasonable agreement. The theoretical pressures shown in figures 9(a) and (b) are lower than the data from the highlight to about $x/X = 0.03$ and higher than the data downstream of $x/X = 0.03$. When the pressures are integrated to obtain cowl drag coefficients, these discrepancies offset each other and reasonable agreement is obtained. Thus, for free-stream Mach numbers below the drag divergence Mach number, the analysis is reasonably accurate in predicting the cowl drag.

Due to the relative proximity of the inlet and boattail, the external cowl pressure distribution could be influenced by the flow over the aft end of the model. This possibility was investigated analytically, and the results are shown in figure 15 for free-stream Mach numbers of 0.60 and 0.75. This figure shows the differences between the cowl drag coefficients for finite inlet-boattail spacings and the cowl drag coefficient for an isolated inlet (no boattail present). These results indicate that reducing the distance between the inlet and the boattail causes a decrease in the cowl drag. For the geometry used in the experimental investigation, the theoretical results indicate that the cowl drag coefficients are lower than those for an isolated inlet by roughly 0.012. This difference is a very weak function of free-stream Mach number and inlet mass-flow ratio. Results are not shown for free-stream Mach 0.85 since results shown in figures 10 and 14 indicate that the theory does not accurately predict the flow over the external cowl at this free-stream Mach number. At a fixed free-stream Mach number and inlet mass-flow ratio, the inlet additive drag was unaffected by variations in l/D_{max}.

Additive drag. - Shown in figure 16 are the effects of mass-flow ratio and free-stream Mach number on the calculated additive drag coefficients. Results obtained using the two-dimensional incompressible potential-flow analysis with the compressibility correction to determine the location of and the pressure distribution along the capture stream tube are shown in figure 16 together with results obtained from one-dimensional

compressible flow theory. The stagnation-point locations for the one-dimensional cal-
culations were those obtained from the two-dimensional analysis. At a given mass-flow
ratio and free-stream Mach number, the two-dimensional additive drag coefficients are
consistently higher than the one-dimensional additive drag coefficients with a difference
of from 0.015 to 0.018 for the mass-flow ratio range of 0.55 to choking and the Mach
number range of 0.60 to 0.85. In an experimental inlet program where instrumentation
is inadequate to accurately determine inlet additive drag, using one-dimensional com-
pressible flow theory to calculate additive drag will give inlet drag values that are too
low.

Inlet net force. - The inlet drag coefficient is equal to the additive drag coefficient
plus the cowl drag coefficient. The theoretical inlet drag coefficients are shown in fig-
ure 17 as a function of mass-flow ratio and free-stream Mach number. The net force on
the inlet changed from a drag at the lower mass-flow ratios to a thrust at the higher
mass-flow ratios. The mass-flow ratio at which the additive drag equaled the cowl suc-
tion force increased with increasing Mach number. If one-dimensional additive drag
values had been used in the calculation of net force, the inlet drag coefficients would be
lower than those shown in figure 17.

SUMMARY OF RESULTS

Incompressible potential-flow calculations, corrected for compressibility effects
using the Lieblein-Stockman compressibility correction, have been performed for the
inlet of a simulator-powered nacelle for free-stream Mach numbers from 0.60 to 0.85
and inlet mass-flow ratios from 0.55 to choking. The internal pressure distributions
obtained using this method were compared with experimental pressure distributions to
determine mass-flow ratios for the experimental program.

Comparisons between theoretical and experimental results allowed the following
observations:

1. Experimental and theoretical internal cowl pressure distributions were in very
good agreement for the first 80 percent of the inlet length at all free-stream Mach num-
bers and for all mass-flow ratios where no local supersonic flow was observed inside
the inlet.

2. External cowl pressure distributions were in good agreement at a free-stream
Mach number of 0.60 for all mass-flow ratios shown. At a free-stream Mach number of
0.75, agreement was good at the choking mass flow but became worse as the mass-flow
ratio was lowered. At a free-stream Mach number of 0.85 agreement was poor at all
mass-flow ratios shown.

3. Stagnation-point locations on the cowl lip agreed reasonably well for the mass-flow ratios and Mach numbers investigated, but the experimental locations were consistently closer to the inlet highlight. The analysis showed no effect of free-stream Mach number on the variation of the stagnation-point location with mass-flow ratio. Experimental data for the Mach number range 0.75 to 0.85 showed the same effect but the data for Mach number 0.60 did not fall on the same curve as the other data.

4. Cowl drag coefficients obtained by integrating the theoretical external pressure distribution decreased with increasing mass-flow ratio for all free-stream Mach numbers. At high mass-flow ratios the theoretical cowl drag coefficients were nearly independent of free-stream Mach number. The theoretical results were in reasonable agreement with data for free-stream Mach numbers of 0.60 to 0.79 but were higher than the data at free-stream Mach number of 0.85.

The theoretical results allowed the following additional observations to be made:

5. The effect of the boundary layer on the pressure distribution both internally and externally was small at the design cruise Mach number (0.75) for the design mass flow and for the choking mass flow. At the design condition the boundary layer caused decreases in local pressure of less than 1 percent with the maximum effect occurring internally just ahead of the fan face.

6. Theoretical additive drag coefficients obtained by integrating the pressure along the calculated capture stream tube were consistently higher than one-dimensional additive drag coefficients at the same free-stream Mach number and mass-flow ratio. The difference between these values was between 0.015 and 0.018 for a mass-flow ratio range of 0.55 to choking and a Mach number range of 0.60 to 0.85.

7. The calculated net external force on the inlet changed from a drag at the lower mass-flow ratios to a thrust at higher mass-flow ratios. The mass-flow ratio at which the additive drag equaled the cowl suction force increased with increasing Mach number.

8. The presence of the boattail in close proximity to the inlet as used in the experimental program caused the cowl drag coefficient to be lower than that for an isolated inlet by roughly 0.012 at free-stream Mach numbers of 0.60 and 0.75.

Lewis Research Center,
    National Aeronautics and Space Administration,
        Cleveland, Ohio, September 12, 1974,
            501-24.

REFERENCES

1. Young, C.: An Investigation of Annular Aerofoils for Turbofan Engine Cowls. RAE-TR-69285, Royal Aircraft Establishment (ARC-R&M-3688), 1969.

2. Re, Richard J.: An Investigation of Several NACA 1-Series Axisymmetric Inlets at Mach Numbers From 0.4 to 1.29. NASA TM X-2917, 1974.

3. Baals, Donald D.; Smith, Norman F.; and Wright, John B.: The Development and Application of High-Critical-Speed Nose Inlets. NACA TR-920, 1948.

4. Shrewsbury, G. D.: Effect of Boattail Juncture Shape on Pressure Drag Coefficients of Isolated Afterbodies. NASA TM X-1517, 1968.

5. Reubush, David E.: Effects of Fineness and Closure Ratios on Boattail Drag of Circular-Arc Afterbody Models With Jet Exhaust at Mach Numbers up to 1.3. NASA TN D-7163, 1973.

6. Tabakoff, Widen; and Sowers, Harry: Drag Analysis of Powered Nacelle Fan Jet Engine Model Test. Z. Flugwiss., vol. 17, no. 4, Apr. 1969, pp. 134-144.

7. Motycka, D. L.; DiSabato, V. J.; and Anderson, L. Q.: The Use of a Powered Model for Subsonic Nacelle Optimization. Paper 72-GT-14, ASME, Mar. 1972.

8. Hess, J. L.; and Smith, A. M. O.: Calculation of Potential Flow About Arbitrary Bodies. Progress in Aeronautical Sciences, Vol. 8, D. Kuchemann, ed., Pergamon Press, 1967, pp. 1-138.

9. Hess, John L.; and Smith, A. M. O.: A General Method for Calculating Low Speed Flows About Inlets. In Aerodynamics of Power Plant Installation, Part 1, AGARDograph-103, Pt. 1, 1965, pp. 345-372.

10. Lieblein, S.; and Stockman, N. O.: Compressibility Correction for Internal Flow Solutions. J. Aircraft, vol. 9, no. 4, Apr. 1972, pp. 312-313.

11. Albers, James A.: Comparison of Predicted and Measured Low-Speed Performance of Two 51-Centimeter-Diameter Inlets at Incidence Angle. NASA TM X-2937, 1973.

12. Albers, James A.: Theoretical and Experimental Internal Flow Characteristics of a 13.97-Centimeter-Diameter Inlet at STOL Takeoff and Approach Conditions. NASA TN D-7185, 1973.

13. Albers, J. A.; and Stockman, N. O.: Calculation Procedures for Potential and Viscous Flow Solutions for Engine Inlets. Paper 74-GT-3, ASME, Mar. 1974.

14. Herring, H. J.; and Mellor, G. L.: Computer Program for Calculating Laminar and Turbulent Boundary Layer Development in Compressible Flow. NASA CR-2068, 1972.

15. Steffen, Fred W.: Cruise Performance of an Isolated 1.15 Pressure Ratio Turbofan Propulsion System Simulator at Mach Numbers from 0.6 to 0.85. NASA TM X-3064, 1974.

16. Wesoky, H. L.; and Steffen, F. W.: Wind Tunnel Tests of a 20 Inch Diameter 1.15 Pressure Ratio Fan Engine Model. Paper 73-1216, AIAA, Nov. 1973.

17. Hancock, J. P.; and Hinson, B. L.: Inlet Development for the L-500. Paper 69-448, AIAA, June 1969.

18. Smith, A. M. O.: Transition, Pressure Gradient, and Stability Theory. Proc. of 9th International Congress of Applied Mechanics, Volume 4 - Boundary Layer, 1957, pp. 234-244.

19. Cebeci, Tuncer; Mosinskis, G. J.; and Smith, A. M. O.: Calculation of Viscous Drag and Turbulent Boundary Layer Separation on Two Dimensional and Axisymmetric Bodies in Incompressible Flows. MDC-JO973-01, McDonnell Douglas Corporation (AD-720775), 1970.

14
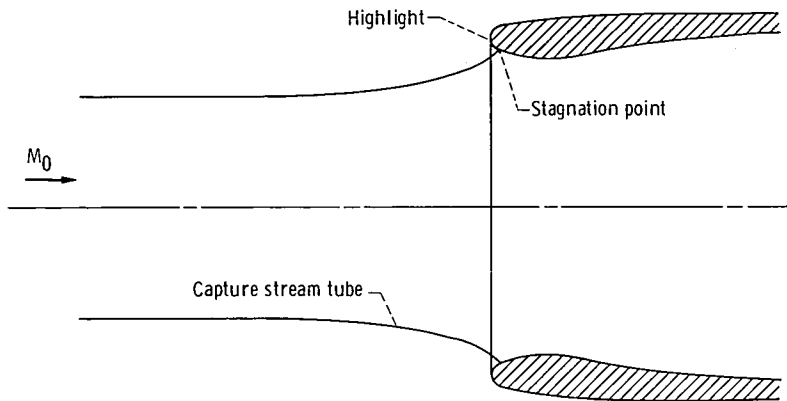
Figure 1. - Inlet at subsonic cruise conditions.
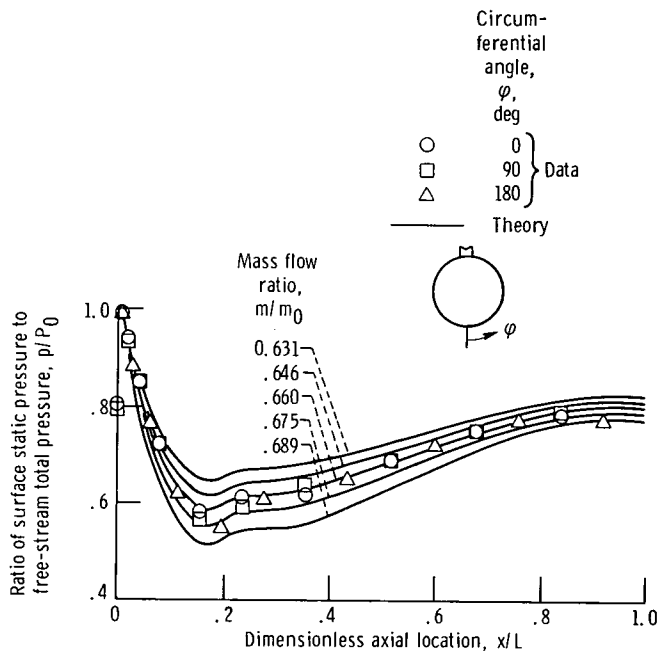
Figure 2. - Application of potential flow results with compressibility correction to determine mass flow ratio. Free-stream Mach 0.75.
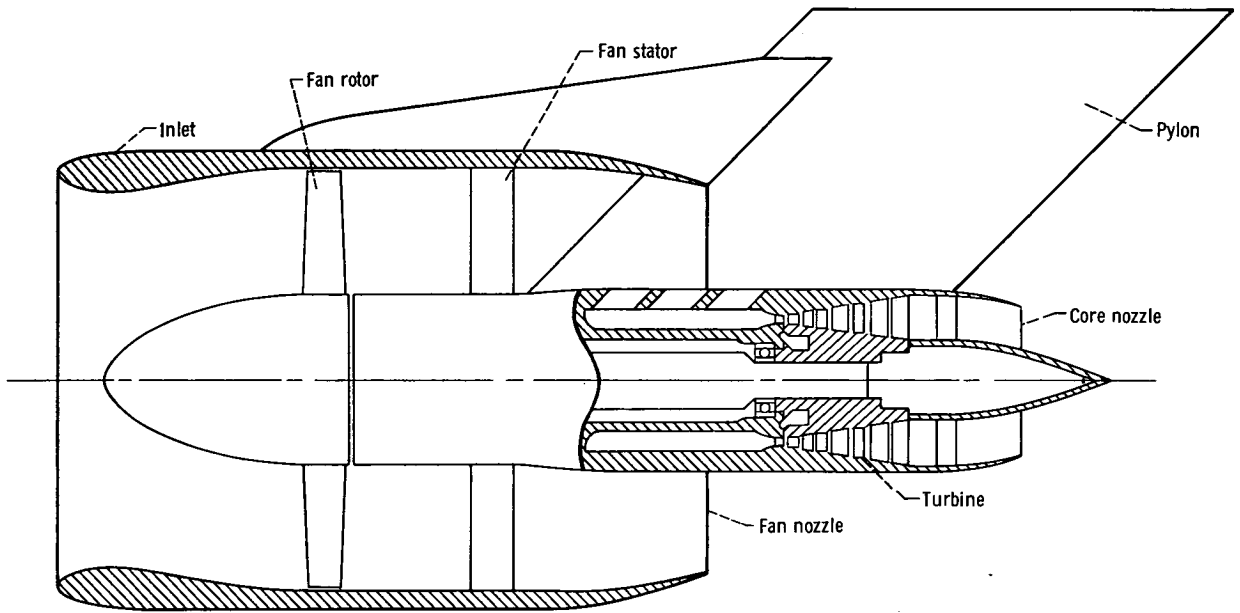
Figure 3. - Simulator powered nacelle (ref. 15).
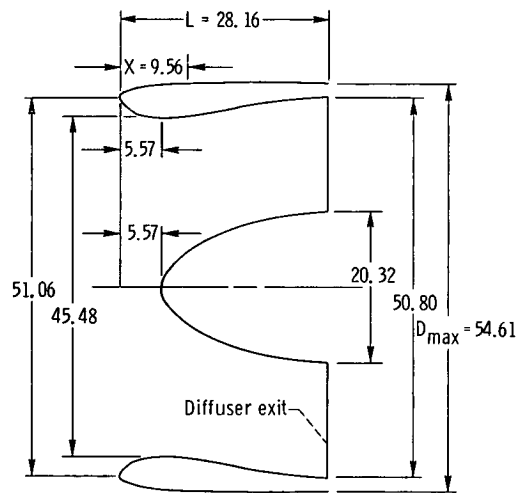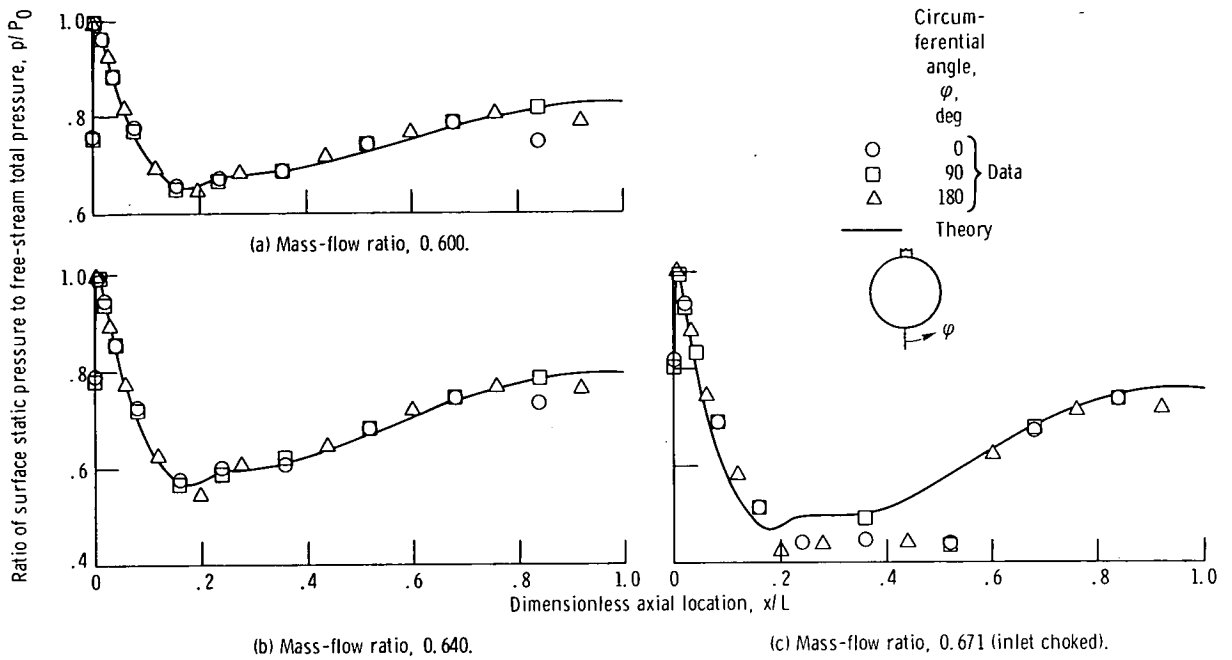

Figure 4. - Inlet geometry. (Dimensions are in cm.)
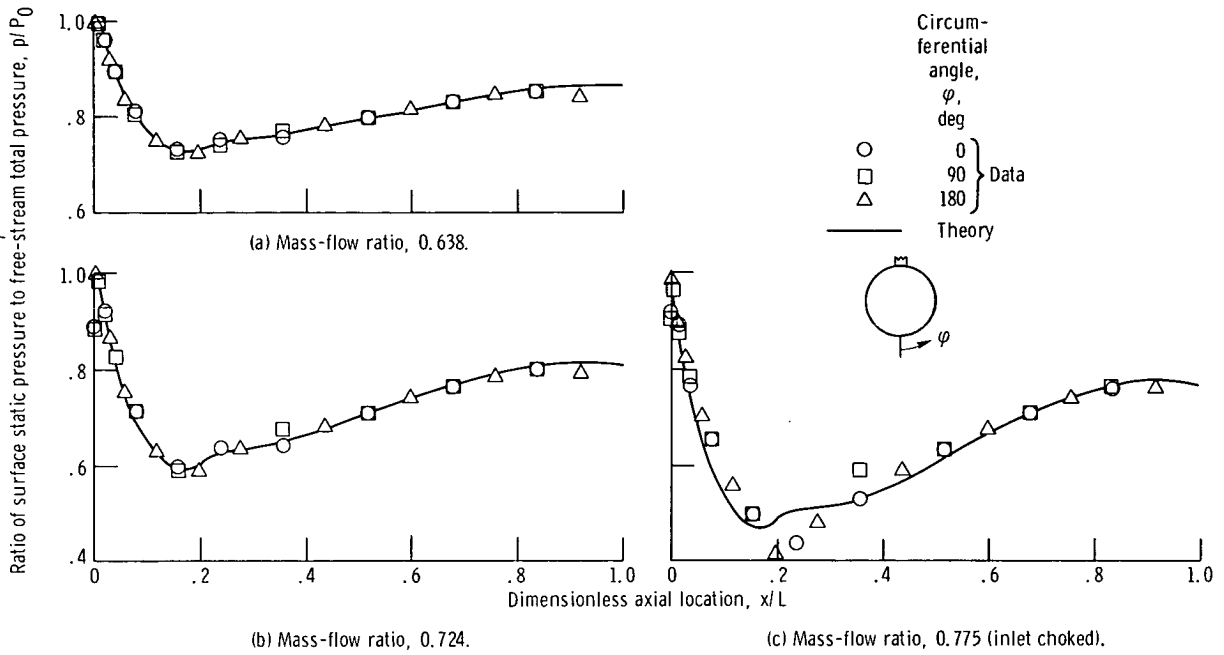
Figure 5. – Comparison of theoretical and experimental cowl internal surface static pressure distributions at free-stream Mach 0.60.
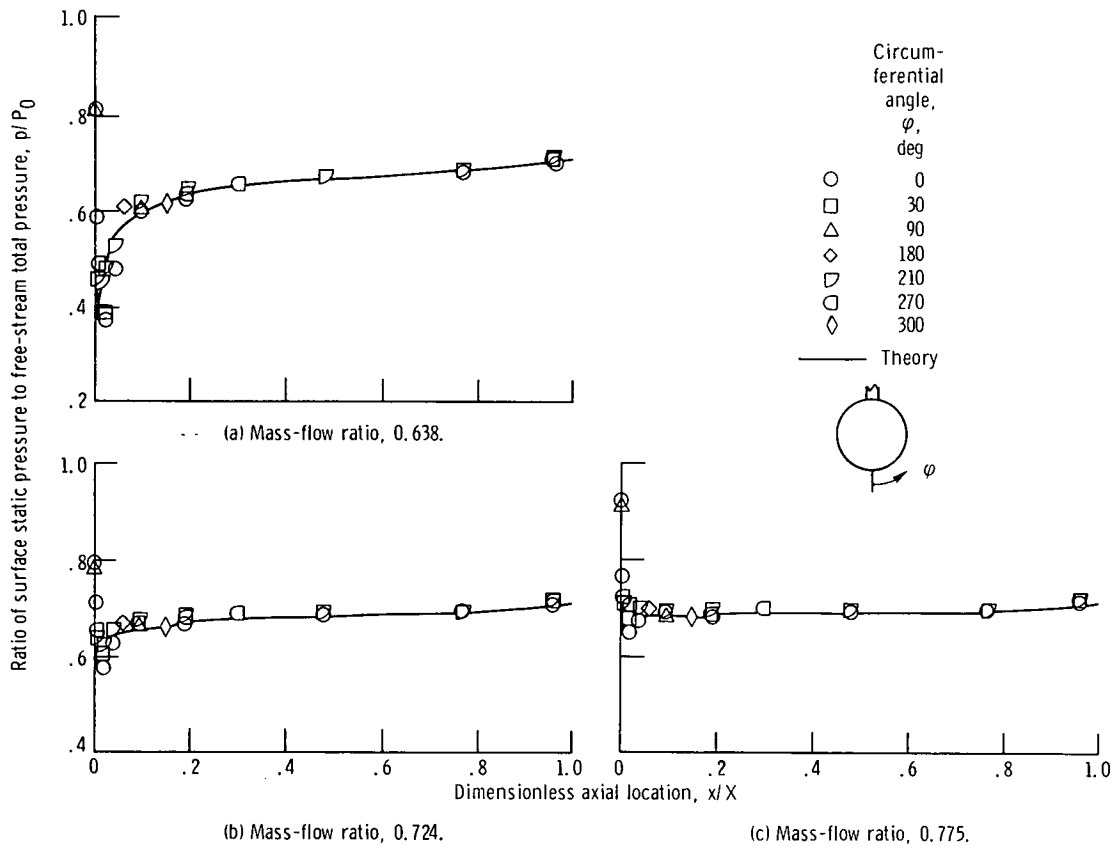
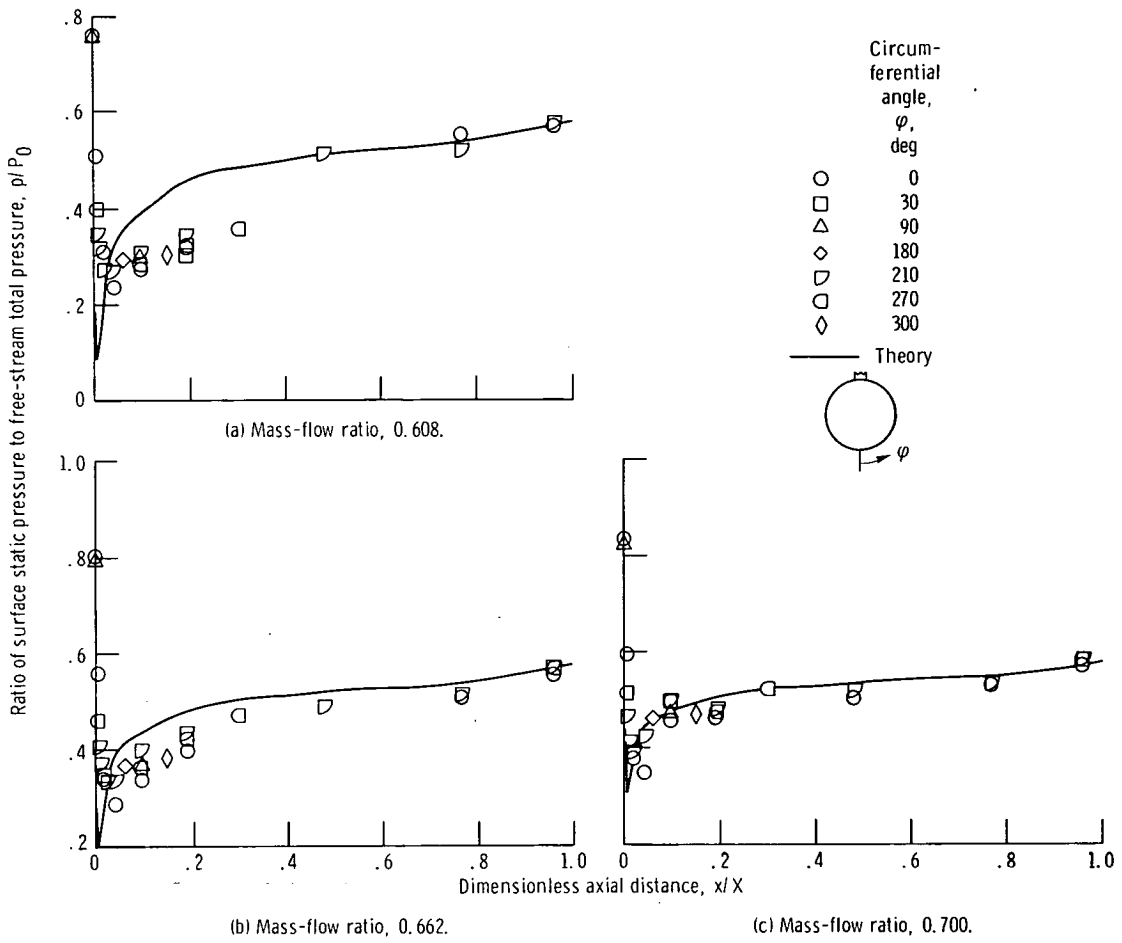(a) Mass-flow ratio, 0.638.

(b) Mass-flow ratio, 0.724.
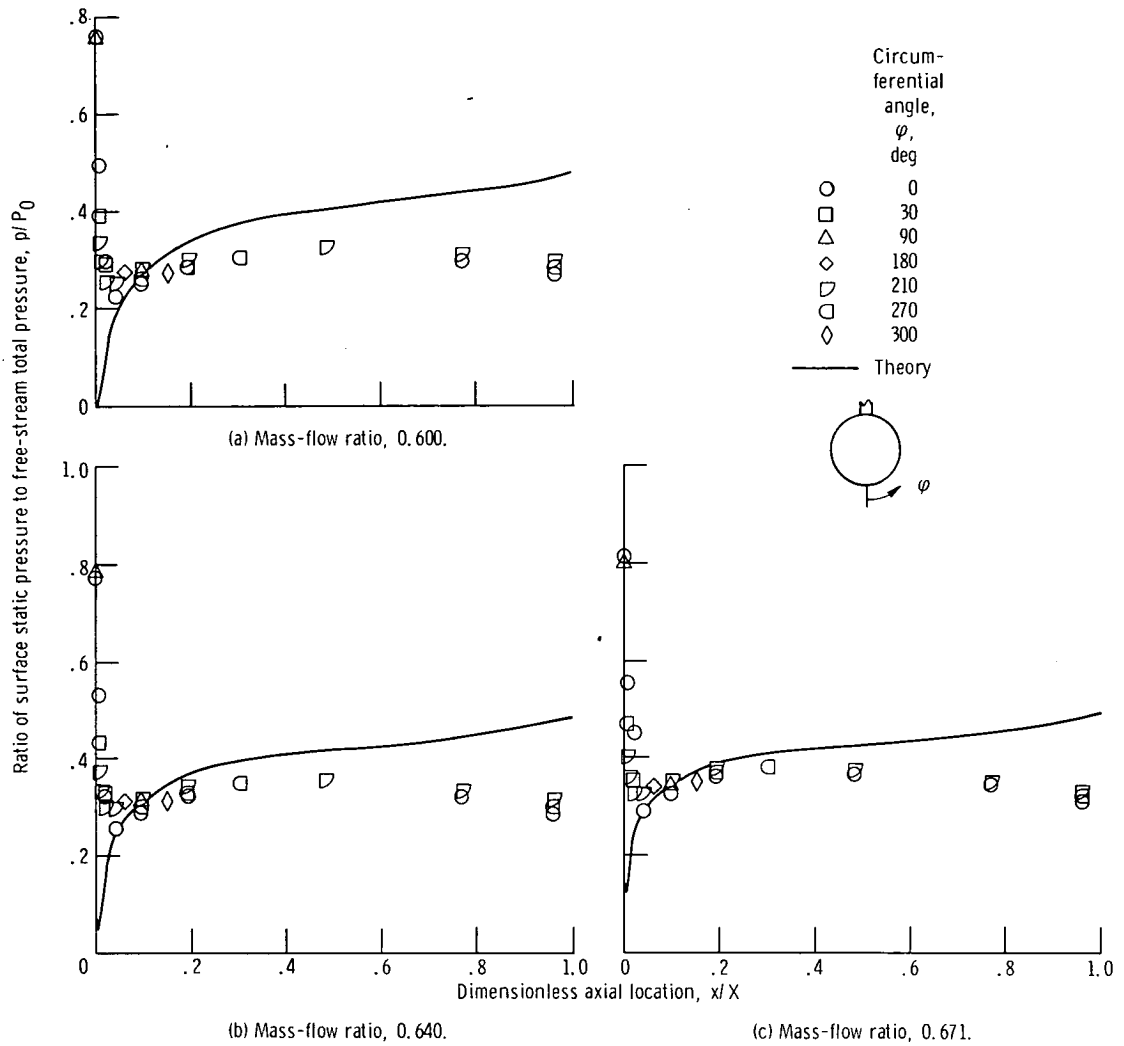
(c) Mass-flow ratio, 0.775 (inlet choked).
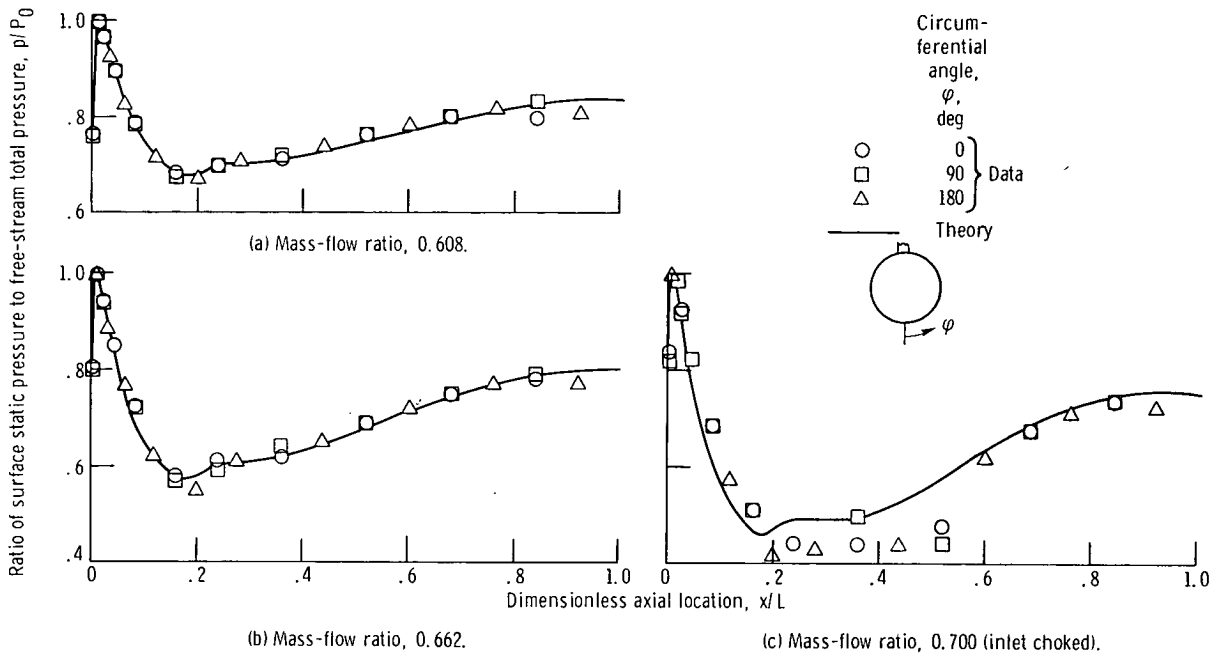
Figure 6. – Comparison of theoretical and experimental cowl internal surface static-pressure distributions at free-stream Mach 0.75.

(a) Mass-flow ratio, 0.608.

(b) Mass-flow ratio, 0.662.
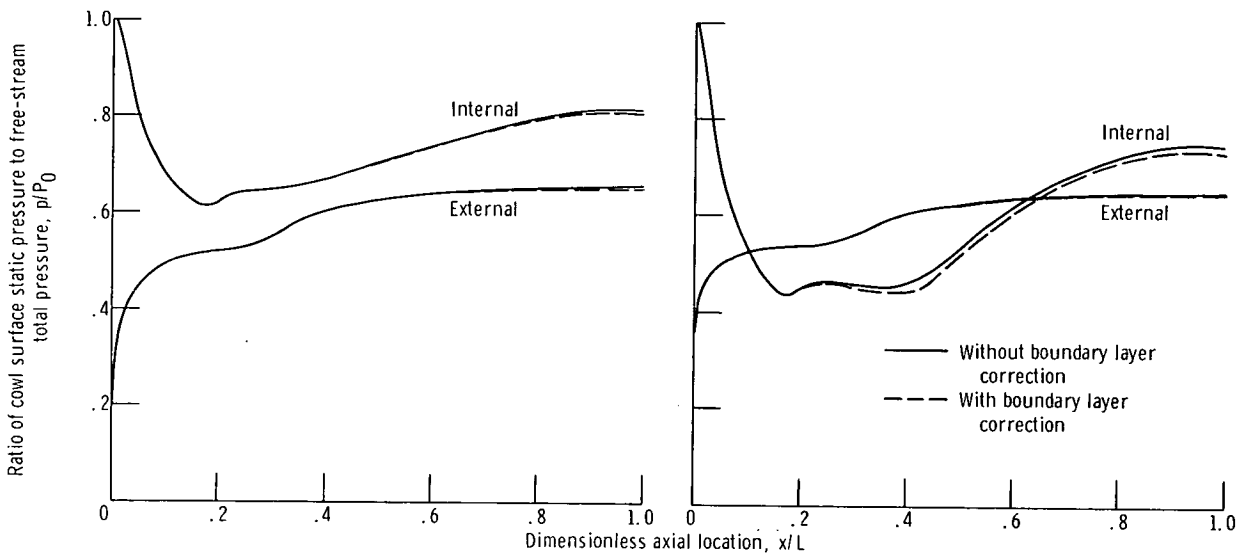
(c) Mass-flow ratio, 0.700 (inlet choked).

Figure 7. - Comparison of theoretical and experimental cowl internal surface static pressure distributions at free-stream Mach 0.85.

(a) Mass-flow ratio, 0.600.

(b) Mass-flow ratio, 0.640.

(c) Mass-flow ratio, 0.671 (inlet choked).

(a) Mass-flow ratio, 0.638.

(b) Mass-flow ratio, 0.724.

(c) Mass-flow ratio, 0.775.

Figure 8. - Comparison of theoretical and experimental cowl external surface static-pressure distributions at free-stream Mach 0.60.

18

Figure 9. – Comparison of theoretical and experimental cowl external surface static-pressure distributions at free-stream Mach 0.75.

Circum-
ferential
angle,
φ,
deg

○	0
□	30
△	90
◇	180
▽	210
◁	270
◇	300
——	Theory

Ratio of surface static pressure to free-stream total pressure, p/P_0

(a) Mass-flow ratio, 0.600.

Dimensionless axial location, x/X

(b) Mass-flow ratio, 0.640.

(c) Mass-flow ratio, 0.671.

Figure 10. – Comparison of theoretical and experimental cowl external surface static-pressure distributions at free-stream Mach 0.85.

20

(a) Mass-flow ratio, 0.645.

(b) Mass-flow ratio, 0.711.

Figure 11. - Effect of boundary layer on theoretical cowl surface static pressure distributions at free-stream Mach 0.75.
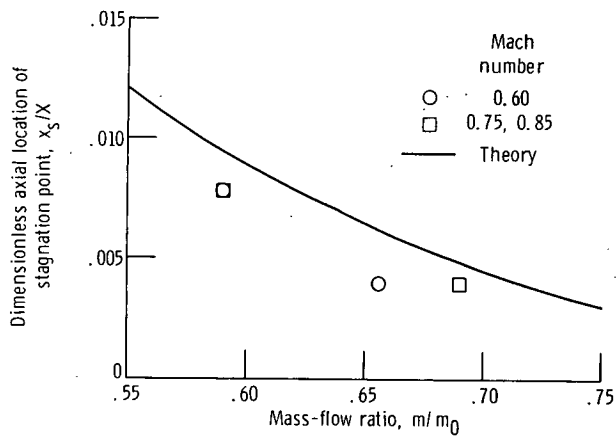
Figure 12. - Effect of mass flow ratio and free-stream Mach number on theoretical and experimental stagnation-point locations. Theoretical and experimental locations are on internal surface of cowl.
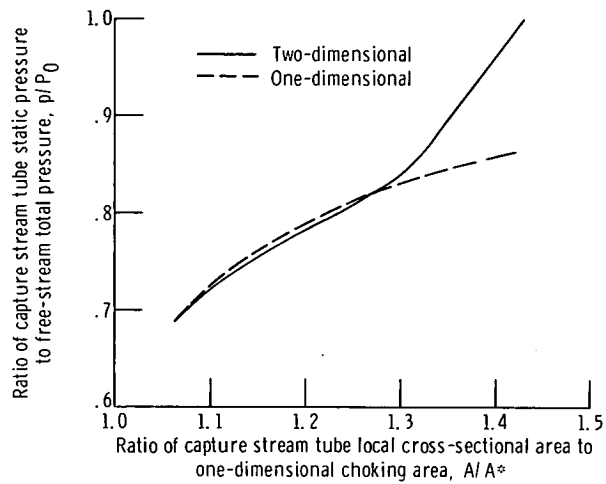
Figure 13. - One- and two-dimensional pressure distri-
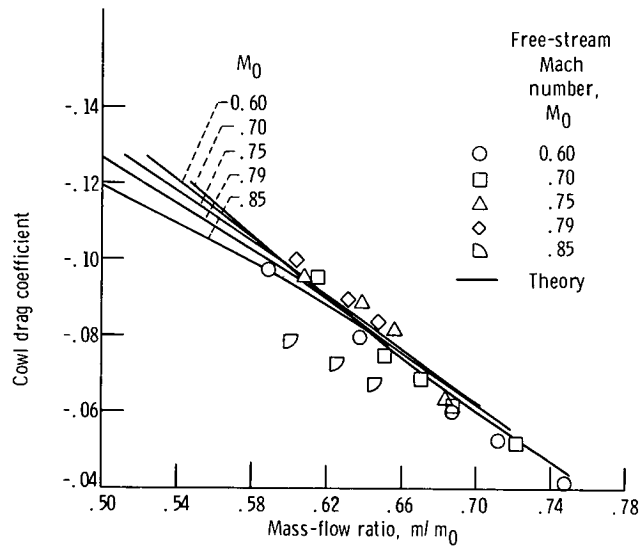butions along capture stream tube. Free-stream
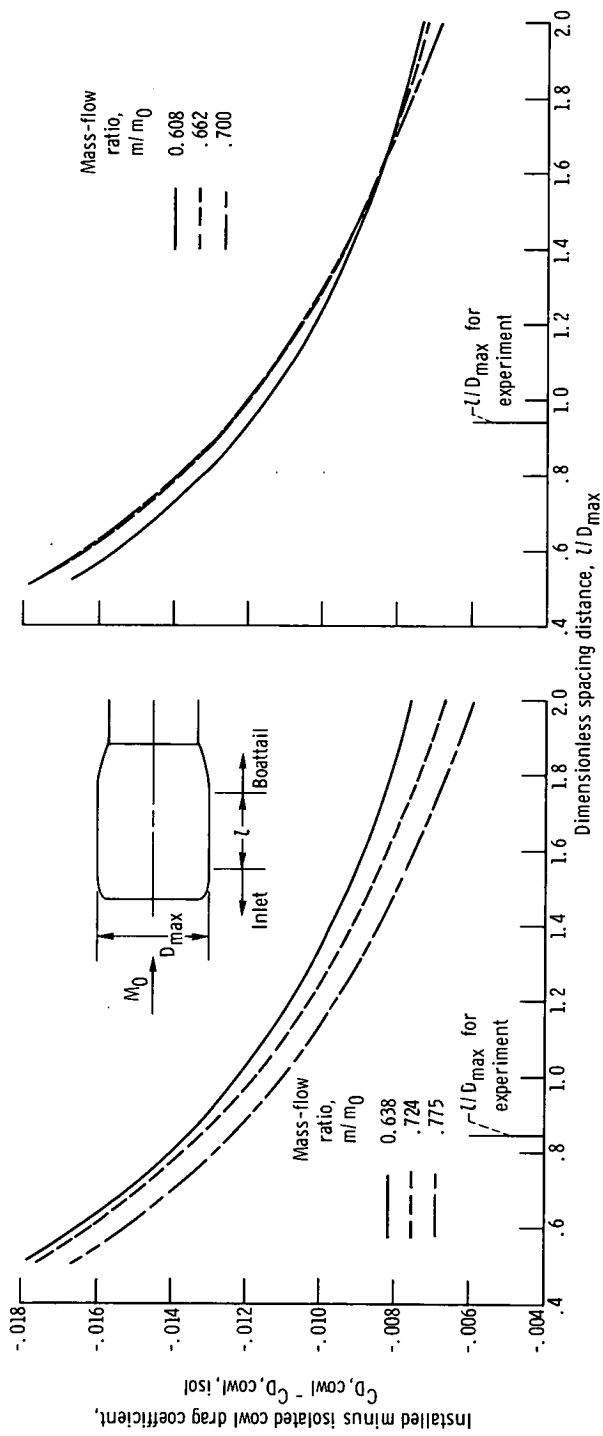Mach, 0.75; mass-flow ratio, 0.608.

Figure 14. - Mass-flow ratio and free-stream Mach number
effects on theoretical and experimental cowl suction
coefficients.

Figure 15. – Effect of inlet-boattail spacing on theoretical cowl drag coefficient.

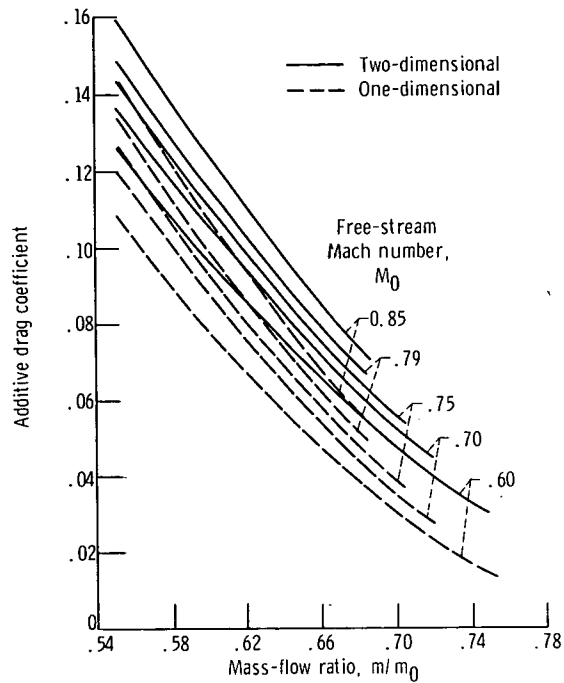(a) Mach 0.60.

(b) Mach 0.75.

Figure 16. - Mass-flow ratio and free-stream Mach number effects on calculated one- and two-dimensional additive drag coefficients.

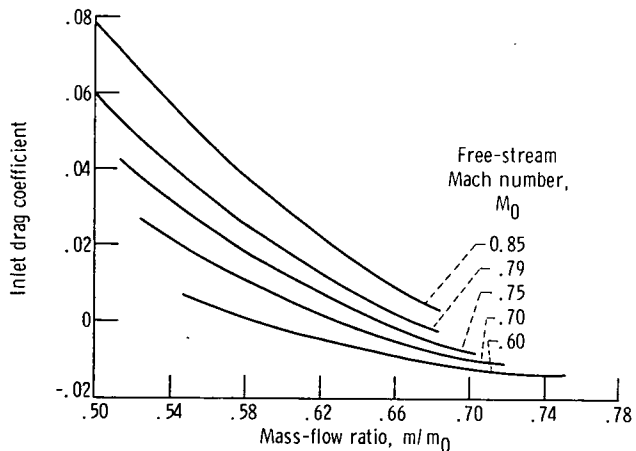Figure 17. - Effects of mass-flow ratio and free-stream Mach number on theoretical inlet drag coefficients.

"The aeronautical and space activities of the United States shall be conducted so as to contribute . . . to the expansion of human knowledge of phenomena in the atmosphere and space. The Administration shall provide for the widest practicable and appropriate dissemination of information concerning its activities and the results thereof."
—NATIONAL AERONAUTICS AND SPACE ACT OF 1958

NASA SCIENTIFIC AND TECHNICAL PUBLICATIONS

TECHNICAL REPORTS: Scientific and technical information considered important, complete, and a lasting contribution to existing knowledge.

TECHNICAL NOTES: Information less broad in scope but nevertheless of importance as a contribution to existing knowledge.

TECHNICAL MEMORANDUMS: Information receiving limited distribution because of preliminary data, security classification, or other reasons. Also includes conference proceedings with either limited or unlimited distribution.

CONTRACTOR REPORTS: Scientific and technical information generated under a NASA contract or grant and considered an important contribution to existing knowledge.

TECHNICAL TRANSLATIONS: Information published in a foreign language considered to merit NASA distribution in English.

SPECIAL PUBLICATIONS: Information derived from or of value to NASA activities. Publications include final reports of major projects, monographs, data compilations, handbooks, sourcebooks, and special bibliographies.

TECHNOLOGY UTILIZATION PUBLICATIONS: Information on technology used by NASA that may be of particular interest in commercial and other non-aerospace applications. Publications include Tech Briefs, Technology Utilization Reports and Technology Surveys.

Details on the availability of these publications may be obtained from:

SCIENTIFIC AND TECHNICAL INFORMATION OFFICE

NATIONAL AERONAUTICS AND SPACE ADMINISTRATION
Washington, D.C. 20546